



Cite this: *Chem. Commun.*, 2024, 60, 7709

Received 1st May 2024,
Accepted 20th June 2024

DOI: 10.1039/d4cc02124j

rsc.li/chemcomm

Intermediates involved in the reduction of SO₂: insight into the mechanism of sulfite reductases†

Aishik Bhattacharya,^{id} Soumya Samanta,^{id} Arnab Kumar Nath, Arnab Ghatak, Somdatta Ghosh Dey* and Abhishek Dey^{id}*

Sulfite reductases (SiRs) catalyze the reduction of SO₃²⁻ to H₂S in biosynthetic sulfur assimilation and dissimilation of sulfate. The mechanism of the 6e⁻/6H⁺ reduction of SO₃²⁻ at the siroheme cofactor is debated, and proposed intermediates involved in this 6e⁻ reduction are yet to be spectroscopically characterized. The reaction of SO₂ with a ferrous iron porphyrin is investigated, and two intermediates are trapped and characterized: an initial Fe(III)–SO₃²⁻ species, which undergoes proton-assisted S–O bond cleavage to form an Fe(III)–SO species. These species are characterized using a combination of resonance Raman (with ³⁴S-labelled SO₂), EPR and DFT calculations. Results obtained help reconcile the different proposed mechanisms for the SiRs.

The reduction of sulfate to sulfide is a crucial step of the geochemical sulfur cycle, which controls biochemical sulfur assimilation and the respiration of sulfate-reducing bacteria.^{1,2} The reduction of sulfate to sulfide is catalyzed by two key metalloenzymes, ubiquitous in microorganisms, including sulfate-reducing bacteria and archaea as well as in methanogens.^{3,4} The reduction of sulfate (SO₄²⁻) requires its insertion into adenosine 5'-monophosphate to form adenosine 5'-phosphosulfate, which is then reduced to release sulfite (SO₃²⁻). SO₃²⁻ is then reduced in the active site of sulfite reductase (SiR). The reduction of sulfite is catalyzed by the siroheme cofactor (Fig. 1A) present in all the SiRs.⁵ The siroheme cofactor is bridged to an Fe₄S₄ cubane *via* one of its cysteine ligands.^{6–8} The mechanism of the 6e⁻ reduction of SO₃²⁻ to S²⁻ is debated. In its active form siroheme and Fe₄S₄ clusters are reduced: *i.e.* the iron in the siroheme is in its Fe(II) state, and the Fe₄S₄ cluster is reduced. Although there are crystal structures of substrate-bound enzyme (Fig. 1A, left), there is no clarity on the oxidation states of the siroheme–Fe₄S₄ unit or sulfur in these structures, and two different mechanisms have been proposed (Fig. 1B).^{9,10} Initially, based on observation of 2e⁻ and 4e⁻

partially reduced species, trithionate and thiosulfate, during SO₃²⁻ reduction, three consecutive 2e⁻/2H⁺ steps were proposed (Fig. 1B).^{11–17} Protons are provided by conserved arginine and lysine residues present in the active site.¹⁵ In addition, a sulfur monoxide (SO)-bound siroheme intermediate was proposed based on the crystal structure obtained by the oxidation of an S²⁻-bound siroheme–Fe₄S₄ site (Fig. 1A right).⁹ Recently, the direct 6e⁻/6H⁺ reduction of SO₃²⁻ in the active site of an SiR (Fig. 1B) was called into question with the identification of a trisulfide formed between the two conserved cysteine residues of another dissimilatory sulfite reductase protein C (DsrC), which is encoded by all

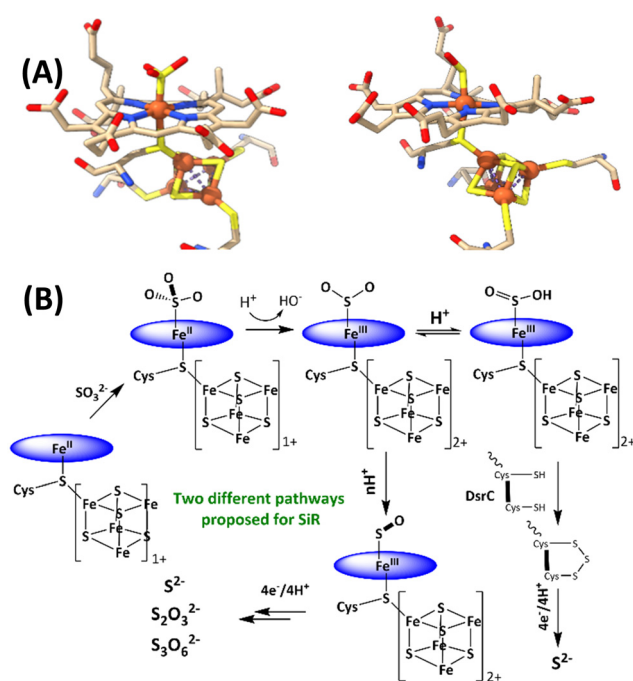


Fig. 1 (A) active sites of SO₃²⁻-bound SiR and SO-bound SiR (pdb id: 7GEP) and (B) proposed mechanisms of the SiRs (direct 6e⁻ reduction and trisulfide pathways are shown). The charge of the [Fe₄S₄] cluster (excluding the cysteines) is indicated next to the cubane.

School of Chemical Sciences Indian Association for the Cultivation of Science, 2A & 2B, Raja SC Mullick Road, Kolkata, West Bengal PIN-700032, India.

E-mail: somdattaghoshdey@gmail.com, abbeyde@gmail.com

† Electronic supplementary information (ESI) available: Experimental methods, additional experimental and computation details are available free of charge in the supporting information. See DOI: <https://doi.org/10.1039/d4cc02124j>

genomes that contain the genes of the catalytic A and B domains of an SiR and binds the DsrAB complex, as an end product of SO_3^{2-} reduction. The rate of SO_3^{2-} reduction by the SiR is first order with respect to the DsrC and about 15 times higher than the rate in the absence of the DsrC.¹⁸ The proposed mechanism invoked the attack on an $\text{Fe(III)}\text{-SO}_2^-/\text{Fe(III)}\text{-SO}_2\text{H}$ species (Fig. 1B), formed after the initial $2e^-$ reduction of SO_3^{2-} , by the two conserved cysteines of the DsrC to form a trisulfide.¹⁹ This trisulfide is then reduced to release sulfide, avoiding generation of trithionate and thiosulfate and resulting in sulfide as the only product of SO_3^{2-} reduction.

A synthetic analogue of the siroheme could be useful in understanding the mechanism.²⁰ Unfortunately, the synthesis of this cofactor is not trivial and has not yet been achieved.^{21,22} Alternatively, simpler porphyrins such as iron tetraphenyl porphyrin (FeTPP), while not an exact model of a siroheme- Fe_4S_4 active site, has a reduction potential similar to that of the siroheme from different enzymes (which vary between -0.19 and -0.29 V at pH 7, and for FeTPP is -0.20 V at pH 7) and hence can be used to gain insight into this intriguing reaction.^{23,24} Initial attempts to investigate the reaction of SO_2 with ferrous porphyrin in non-polar organic solvents inevitably resulted in the formation of sulfate-bound ferric porphyrin.^{21,25-27} Recently, the reaction of ferrous tetraphenyl porphyrin with SO_2 was investigated in a protic organic solvent at room temperature (RT). The reaction proceeded to result in the $2e^-$ reduction of SO_2 to SO , and the released SO could be trapped using 2,3-dimethylbutadiene, resulting in the formation of a cyclic sulfoxide.²⁸ An $\text{Fe(III)}\text{-SO}$ intermediate was identified and was characterized using Mössbauer and EPR spectroscopy as a low-spin ferric porphyrin antiferromagnetically coupled to a triplet SO , resulting in an $S = 1/2$ species. Although the presence of the Fe-S bond could not be established experimentally, the observed S-O vibrations of this species were consistent with theoretically predicted vibrations for an $\text{Fe(III)}\text{-SO}$ species.²⁸ One of the $2e^-$ needed is derived from iron porphyrin to which SO is bound, and the other comes from a free Fe(II)TPP . The 1:1 ratio of $[\text{Fe(III)TPP}]^+$ and $[\text{Fe(III)TPP-SO}]^+$ species was confirmed by Mössbauer spectroscopy.^{24,26} The $\text{Fe(III)}\text{-SO}_2^-/\text{Fe(III)}\text{-SO}_2\text{H}$ species, proposed in the SiR mechanism, has not however been observed either in the protein or in synthetic systems.

To assess the involvement of any intermediate species prior to the $[\text{Fe(III)TPP-SO}]^+$ species, the reaction of Fe(II)TPP with SO_2 is allowed to proceed at -80°C (MeOH-liq. N_2 bath) for 10 min, and then, the reaction mixture is frozen in liq. N_2 . New EPR signals (Fig. 2A, green) are obtained with $g = 2.36, 2.27,$ and 1.89 , indicating the formation of another $S = 1/2$ low-spin intermediate species (henceforth referred to as Int-I) prior to the formation of $[\text{Fe(III)}\text{-SO}]^+$ species (henceforth referred to as Int-II). In parallel to the Int-I signals, there is a $g = 6.0$ signal corresponding to a high-spin $[\text{Fe(III)TPP}]^+$ species, suggesting that Int-I also results from the $2e^-$ reduction of SO_2 , where one electron is derived from Fe(II)TPP to which SO_2 to, and the other electron is derived from a free Fe(II)TPP , which gets oxidized to a high-spin $[\text{Fe(III)TPP}]^+$ species with a $g = 6.0$ EPR signal. Mössbauer data suggests an equal population of these two species in the sample (Fig. S1, ESI[†]). When the solution is warmed up to -40°C (10 min), the EPR

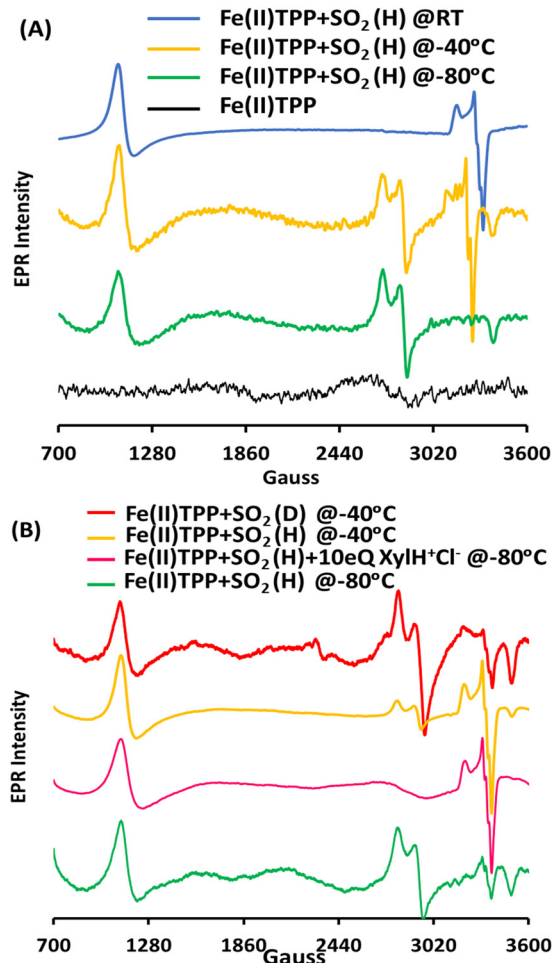


Fig. 2 (A) X-band EPR data collected at 77 K for a frozen solution of Fe(II)TPP (black), reaction mixture of Fe(II)TPP and SO_2 in THF with 1%MeOH (v/v) kept at -80°C for 10 min and later frozen in liq. N_2 (green), kept at -40°C for 10 min and later frozen in liq. N_2 (yellow) and kept at RT for 10 min and further frozen in liq. N_2 (blue, from reference 27). (B) Reaction mixture of $\text{Fe(II)TPP} + \text{SO}_2$ in THF with 1%MeOH (v/v) kept at -80°C for 10 min and later frozen in liq. N_2 (green); reaction mixture of $\text{Fe(II)TPP} + \text{SO}_2$ in THF with 1%MeOH (v/v) and 10 eq. of XylH^+Cl^- kept at -80°C for 10 min and later frozen in liq. N_2 (pink), kept at -40°C for 10 min and further frozen in liq. N_2 (yellow); and $\text{Fe(II)TPP} + \text{SO}_2$ reaction mixture in THF with 1%MeOH (v/v) kept at -40°C for 10 min and later frozen in liq. N_2 (red).

signals originating from Int-I decrease, and the EPR signals from Int-II emerge (Fig. 2A, yellow), indicating that Int-I decays to produce Int-II (Fig. 2A, blue), *i.e.*, Int-I is a species formed prior to Int-II in the reaction.

The transition of Int-I to Int-II depends on the availability of the protons. When the reaction of SO_2 and Fe(II)TPP is performed at -80°C (10 min) but in the presence of 10 eq. of xylidinium chloride (XylH^+Cl^-) as a proton source, the EPR signals from Int-I (Fig. 2B, green) are no longer observed and only those of Int-II are observed (Fig. 2B, pink). Similarly, when the MeOH proton source in the solution is deuterated (1% CD_3OD instead of 1% MeOH, CD_3OD represented as MeOD) and instead used as the proton source, the EPR signal of the reaction at -40°C (Fig. 2B, red) shows Int-I and Int-II in a 5:1 ratio relative to MeOH where this ratio is 1:2, indicating that there is an H/D isotope effect in the

conversion of Int-I to Int-II, consistent with a protonation step being involved in the reaction.

Int-I trapped at -80°C is further characterized using resonance Raman spectroscopy of samples prepared with SO_2 and comparing the vibrations with those observed when $^{34}\text{SO}_2$ is used. In Int-I, vibration is observed at 984 cm^{-1} , which shifts to 970 cm^{-1} on ^{34}S substitution (Fig. 3A, top). This is consistent with an S–O stretching mode from an SO_2 -derived axial ligand.^{29,30} In the lower energy region, vibration is observed at 340 cm^{-1} , which shifts to 337 cm^{-1} on ^{34}S labelling (Fig. 3B, bottom). The energy of this vibration and isotope shift indicate that it is an Fe–S stretching mode.^{31,32}

In the past, Int-II had been tentatively assigned as a solvent-bound $[\text{Fe}(\text{III})\text{TPP-SO}]^+$ species with the S–O vibration at 1014 cm^{-1} , which falls on the shoulder of a porphyrin band at 1004 cm^{-1} . Accordingly, the 1014 cm^{-1} vibration shifts to 1005 cm^{-1} (Fig. 4A, top) on ^{34}S substitution, confirming it to be an S–O stretching vibration, as previously assigned. The Fe–S vibration of Int-II is observed at 382 cm^{-1} , which shifts to 377 cm^{-1} with ^{34}S substitution (Fig. 4B, bottom). There is also another vibration at 206 cm^{-1} , which shifts to 204 cm^{-1} with ^{34}S (Fig. 4B, bottom) which may very well result from mixing of the Fe–S mode with a porphyrin vibration. There is some residual Fe–S vibration at 340 cm^{-1} from Int-I (Fig. 4B, bottom). Thus, the Fe–S and S–O vibrations, confirmed with ^{34}S labelling, clearly indicate that Int-I and Int-II have Fe–S and S–O bonds. Samples prepared with MeOD did not show any shift in any of the S–O or Fe–S vibrations, suggesting that none

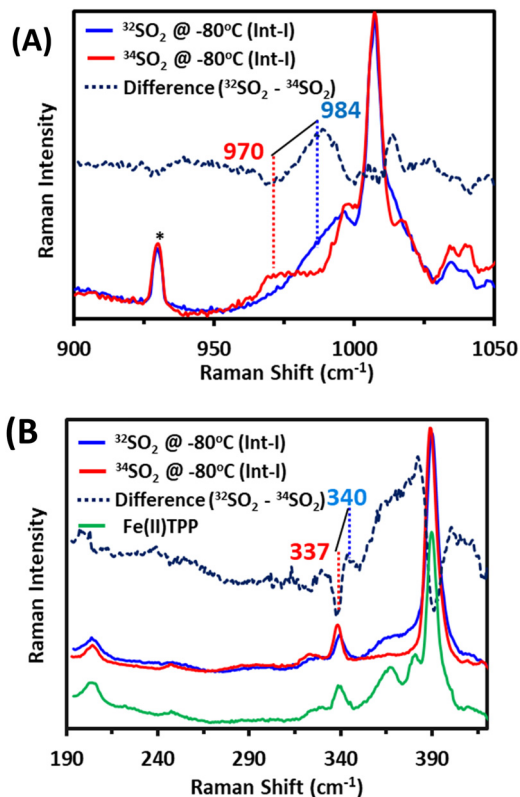


Fig. 3 Resonance Raman data on a frozen solution of Int-I (A) S–O region and (B) Fe–S region. 413.1 nm excitation and 10 mW laser power, prepared with $^{32}\text{SO}_2$ (blue traces) and $^{34}\text{SO}_2$ (red traces). The $^{32}\text{SO}_2$ sample contains some unreacted $\text{Fe}(\text{II})\text{TPP}$ (green). *Indicates a solvent peak.

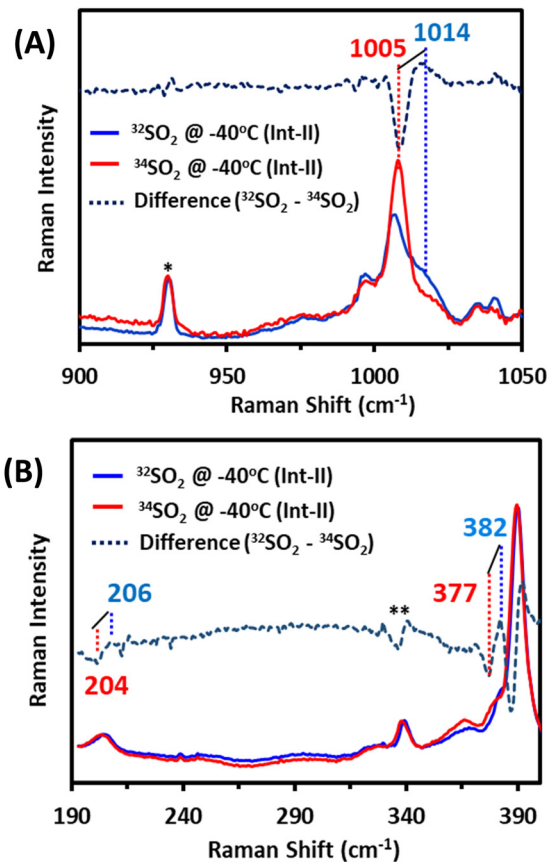
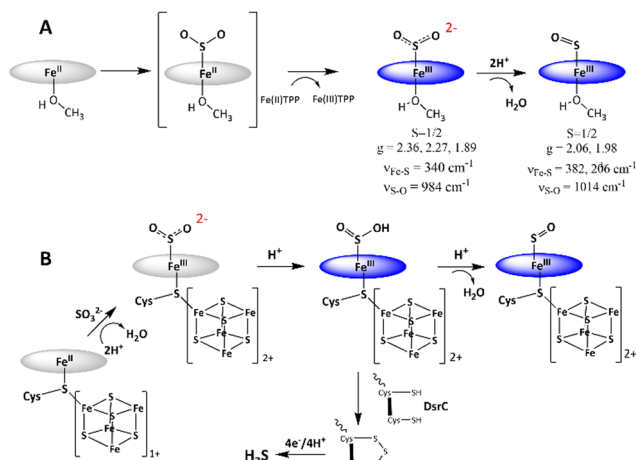


Fig. 4 Resonance Raman data on a frozen solution of Int-II (A) S–O region and (B) Fe–S region. 413.1 nm excitation and 10 mW laser power, prepared with $^{32}\text{SO}_2$ (blue traces) and $^{34}\text{SO}_2$ (red traces). *Indicates a solvent peak and ** represents residual Int-I.

of the species are likely to be protonated. Density functional theory (DFT) calculations are used to gain further insight.

DFT calculations are used to compute the hypothetical structure of possible intermediates in the reduction of SO_2 to SO by $\text{Fe}(\text{II})\text{TPP}$.^{33,34} The DFT method being used was reported to reproduce the Mössbauer and vibrational spectroscopy data of the $[\text{Fe}(\text{III})\text{-SO}]^+$ species quite well.²⁸ EPR data indicates that Int-I and Int-II are $S = 1/2$ $\text{Fe}(\text{III})$ species, and the presence of a free $[\text{Fe}(\text{III})\text{TPP}]^+$ indicates that SO_2 is reduced by $2e$ to its formal +2 oxidation state in both these species. Additionally, conversion of Int-I to Int-II requires a proton, as indicated by the EPR data obtained with MeOD and XylH^+Cl^- . The most likely description of Int-I is $[\text{Fe}(\text{III})\text{TPP-SO}_2]^-$ and Int-II has already been proposed to be $[\text{Fe}(\text{III})\text{TPP-SO}]^+$. The possibility of the formation of $\text{Fe}(\text{III})\text{TPP-SO}_2\text{H}$ is removed by the lack of an H/D isotope effect in the S–O vibration. The DFT-calculated structure of an $S = 1/2$ $[\text{Fe}(\text{III})\text{TPP-SO}_2]^-$ with an axial MeOH (from the solvent) shows an Fe–S bond length of 2.33 \AA and an S–O bond length of 1.50 \AA (Table S1, ESI†). The computed S–O bond length shows a substantial increment from the reported 1.44 \AA bond length of SO_2 and is closer to that computed for free SO_2^- (one-electron-reduced SO_2) consistent with the reduction of SO_2 .^{35,36} The Fe–S stretching vibration is computed to be at 339 cm^{-1} , which shifts to 337 cm^{-1} on ^{34}S substitution. The



Scheme 1 (A) Mechanism of SO_2 reduction observed for Fe(II)TPP . Spectroscopic parameters are indicated below the proposed structures of the intermediates. (B) Mechanism of the SiR is refined based on the mechanism of SO_2 reduction observed for Fe(II)TPP . The porphyrin ligand is indicated as a blue circle for clarity.

symmetric S–O vibration is calculated to be at 994 cm^{-1} , which shifts by 7 cm^{-1} on ^{34}S substitution to 987 cm^{-1} . Computed Fe–S and S–O vibrations, and their shifts on ^{34}S substitution are in excellent agreement with values obtained experimentally (Table S1, ESI[†]). Note that the S–O vibration of free SO_2 is at 1156 cm^{-1} , which, as expected, is higher than that of $[\text{Fe(III)TPP-SO}_2]^-$ species, as reduction of SO_2 is expected to weaken the S–O vibration. Analysis of the wavefunction of the $[\text{Fe(III)TPP-SO}_2]^-$ species reveals very covalent interaction between Fe and SO_2 , and the dominant bonding interaction is the σ bond between the unoccupied d_z^2 orbital of the iron and occupied $\text{SO}_2^{2-} \pi^*$ orbital (Fig. S2, ESI[†]).

The mechanism of SO_2 reduction by Fe(II)TPP (Scheme 1A) thus involves a $2e^-$ step, resulting in SO_2^{2-} species bound to $[\text{Fe(III)TPP}]^+$ to form $[\text{Fe(III)TPP-SO}_2]^-$ Int-I, like the mechanism proposed for the SiR by Pereira and co-workers.¹⁸ No $1e^-$ -reduced intermediate could be observed even at -80°C , rather an additional electron is derived from a free Fe(II)TPP to result in a $2e^-$ reduction, which substitutes for the reduced $[\text{Fe}_4\text{S}_4]^+$ cluster at the SiR active site. Protonation of this species leads to the cleavage of the S–O bond and formation of the $[\text{Fe(III)TPP-SO}]^+$ species, Int-II. The reaction can proceed even at -40°C with a weak proton source such as MeOH, albeit it is accelerated in the presence of XylH^+Cl^- . This indicates that the pK_a of $[\text{Fe(III)TPP-SO}_2]^-$ is higher than that of MeOH in THF. Thus, the $2e^-$ -reduced intermediate in the active site of an SiR, which has several arginine and lysine residues, is most likely to be $\text{Fe(III)-SO}_2\text{H}$. The reaction mechanism observed here suggests that the most likely mechanism of an SiR (Scheme 1B) involves the initial formation of the $\text{Fe(III)-SO}_2\text{H}$ species (Scheme 1B) after the $2e^-$ reduction of SO_2 .¹⁸ The structure of the DsrC bound to the SiR shows that cysteinyl sulfur from the DsrC is less than 2 \AA away from the siroheme, and the faster step is likely to be the attack of the cysteines of the DsrC protein resulting in the trisulfide.^{18,19}

The research is sponsored by the Department of Science and Technology, India SERB grant CRG/2021/000154.

Data availability

The data supporting this article have been included as part of the ESI[†].

Conflicts of interest

There are no conflicts to declare.

Notes and references

- G. D. Fauque, in *Ecology of Sulfate-Reducing Bacteria*, ed. L. L. Barton, Springer US, Boston, MA, 1995, pp. 217–241.
- J. Simon and P. M. H. Kroneck, in *Advances in Microbial Physiology*, ed. R. K. Poole, Academic Press, 2013, vol. 62, pp. 45–117.
- M. Jespersen, A. J. Pierik and T. Wagner, *Nat. Chem. Biol.*, 2023, **19**, 695–702.
- M. Jespersen and T. Wagner, *Nat. Microbiol.*, 2023, **8**, 1227–1239.
- M. J. Murphy, L. M. Siegel, S. R. Tove and H. Kamin, *Proc. Natl. Acad. Sci. U. S. A.*, 1974, **71**, 612–616.
- B. R. Crane, L. M. Siegel and E. D. Getzoff, *Science*, 1995, **270**, 59–67.
- J. A. Christner, E. Münck, P. A. Janick and L. M. Siegel, *J. Biol. Chem.*, 1981, **256**, 2098–2101.
- I. Askenasy and M. E. Stroupe, in *Transition Metals and Sulfur – A Strong Relationship for Life*, ed. M. E. Sosa Torres and P. M. H. Kroneck, Metal Ions in Life Sciences, De Gruyter, Berlin, Boston, 2020, vol. 20, ch. 10, pp. 343–380.
- B. R. Crane, L. M. Siegel and E. D. Getzoff, *Biochemistry*, 1997, **36**, 12120–12137.
- P. A. Janick, D. C. Rueger, R. J. Krueger, M. J. Barber and L. M. Siegel, *Biochemistry*, 1983, **22**, 396–408.
- K. Parey, E. Warkentin, P. M. H. Kroneck and U. Ermler, *Biochemistry*, 2010, **49**, 8912–8921.
- J. M. Akagi, *Biochem. Biophys. Res. Commun.*, 1983, **117**, 530–535.
- H. L. Drake and J. M. Akagi, *J. Bacteriol.*, 1977, **132**, 139–143.
- H. L. Drake and J. M. Akagi, *J. Bacteriol.*, 1976, **126**, 733–738.
- K. W. Smith and M. E. Stroupe, *Biochemistry*, 2012, **51**, 9857–9868.
- M. Surducian, A. M. V. Brănzanic and R. Silaghi-Dumitrescu, *Int. J. Quantum Chem.*, 2018, **118**, e25697.
- A. M. V. Brănzanic, U. Ryde and R. Silaghi-Dumitrescu, *J. Inorg. Biochem.*, 2020, **203**, 110928.
- A. A. Santos, S. S. Venceslau, F. Grein, W. D. Leavitt, C. Dahl, D. T. Johnston and I. A. C. Pereira, *Science*, 2015, **350**, 1541–1545.
- T. F. Oliveira, C. Vonnrhein, P. M. Matias, S. S. Venceslau, I. A. C. Pereira and M. Archer, *J. Biol. Chem.*, 2008, **283**, 34141–34149.
- A. M. V. Brănzanic, U. Ryde and R. Silaghi-Dumitrescu, *Chem. Commun.*, 2019, **55**, 14047–14049.
- L. Cai and R. H. Holm, *J. Am. Chem. Soc.*, 1994, **116**, 7177–7188.
- C. Zhou, L. Cai and R. H. Holm, *Inorg. Chem.*, 1996, **35**, 2767–2772.
- M. Hirasawa, M. Nakayama, T. Hase and D. B. Knaff, *Biochim. Biophys. Acta Bioenerg.*, 1608, **2004**, 140–148.
- S. Bhunia, A. Ghatak, A. Rana and A. Dey, *J. Am. Chem. Soc.*, 2023, **145**, 3812–3825.
- A. M. Stolzenberg, S. H. Strauss and R. H. Holm, *J. Am. Chem. Soc.*, 1981, **103**, 4763–4778.
- W. R. Scheidt, Y. J. Lee and M. G. Finnegan, *Inorg. Chem.*, 1988, **27**, 4725–4730.
- P. Cocolios, G. Lagrange, R. Guilard, H. Oumous and C. Lecomte, *J. Chem. Soc., Dalton Trans.*, 1984, 567–574.
- A. Bhattacharya, A. Kumar Nath, A. Ghatak, A. Nayek, S. Dinda, R. Saha, S. Ghosh Dey and A. Dey, *Angew. Chem., Int. Ed.*, 2023, **62**, e202215235.
- H. G. Houlton and H. V. Tartar, *J. Am. Chem. Soc.*, 1938, **60**, 544–548.
- J. R. Durig, L. Zhou, T. Schwartz and T. Gounef, *J. Raman Spectrosc.*, 2000, **31**, 193–202.
- A. C. Mot, C. Bischin, G. Damian, A. A. Attia, E. Gal, N. Dina, N. Leopold and R. Silaghi-Dumitrescu, *J. Inorg. Biochem.*, 2018, **179**, 32–39.
- A. Rana, S. Amanullah, P. K. Das, A. B. McQuarters, N. Lehnert and A. Dey, *J. Am. Chem. Soc.*, 2019, **141**, 5073–5077.
- A. D. Becke, *J. Chem. Phys.*, 1993, **98**, 5648–5652.
- C. Lee, W. Yang and R. G. Parr, *Phys. Rev. B: Condens. Matter Mater. Phys.*, 1988, **37**, 785–789.
- I. Jana, S. Naskar, M. Das and D. Nandi, *Eur. Phys. J. D*, 2019, **73**, 233.
- E. Krishnakumar, S. V. K. Kumar, S. A. Rangwala and S. K. Mitra, *J. Phys. B: At., Mol. Opt. Phys.*, 1996, **29**, L657.